The most extreme rainfall erosivity event ever recorded in China: The "7.20" storm in Henan province

Yuanyuan Xiao[1], Shuiqing Yin[1], Bofu Yu[2], Conghui Fan[1], Wenting Wang[1], Yun Xie[1]

[1]State Key Laboratory of Earth Surface Processes and Resource Ecology, Faculty of Geographical Science, Beijing Normal University, Beijing, 100875, China
[2]Australian Rivers Institute, School of Engineering and Built Environment, Griffith University, Nathan, Queensland, QLD 4111, Australia

Correspondence to: Shuiqing Yin (yinshuiqing@bnu.edu.cn)

Abstract. Severe water erosion occurs during extreme storm events. Such an exceedingly severe storm occurred in Zhengzhou in central China on 20 July 2021 (the "7.20" storm). The magnitude and frequency of occurrence of this storm event were examined in terms of how erosive it was. To contextualize this extreme event, hourly rainfall data from 2420 automatic meteorological stations in China from 1951 to 2021 were analyzed to: (1) characterize the spatial and temporal distribution of rainfall amount and rainfall erosivity of the "7.20" storm, (2) evaluate the average recurrence interval of the maximum daily and event rainfall erosivity, and (3) establish the geographical distribution of the maximum daily and event rainfall erosivity in China. The center of the "7.20" storm moved from southeast to northwest in Henan province, and the most intense period of rainfall occurred in the middle and late stages of the storm. Zhengzhou meteorological station happened to be aligned with the center of the storm, with a maximum daily rainfall of 552.5 mm and a maximum hourly rainfall intensity of 201.9 mm·h^{-1}. The average recurrence intervals of the maximum daily rainfall erosivity (43,354 MJ·mm·ha^{-1}·h^{-1}) and the maximum event rainfall erosivity (58,874 MJ·mm·ha^{-1}·h^{-1}) were estimated to be about 10,000 and 23,100 years, respectively, assuming the log Pearson type III distribution, and these were the maximum rainfall erosivity ever recorded among 2420 meteorological stations in mainland China. The "7.20" storm suggests that the most erosive of storms does not necessarily occur in the wettest places in southern China, and it can occur in mid-latitude around 35 °N with a moderate mean annual rainfall of 566.7 mm in Zhengzhou.

Keywords. soil erosion, extreme rainfall, rainfall erosivity, the return period

1 Introduction

Soil erosion ~~a~~is a land degradation process that can affect food production, biodiversity, carbon stocks and ecosystem services (Kebede et al. 2021; Panagos et al., 2015). Soil erosion models are powerful tools to evaluate the rate of erosion and the effect of soil and water conservation measures for decision makers. The Universal Soil Loss Equation (USLE) (Wischmeier and Smith, 1965, 1978) and the revised USLE (Renard et al., 1997; USDA–ARS, 2013), and the Chinese Soil Loss Equation (CSLE, Liu et al., 2002) are widely used empirical soil erosion prediction models for estimating the long-term average amount of soil loss. Rainfall erosivity quantifies the potential ability of rainfall and runoff to erode the soil and represents the climatic effect on soil erosion as one of the factors in the USLE, RUSLE and CSLE (Yin et al., 2017).

Most studies have focused on the long-term average of rainfall and rainfall erosivity characteristics (Gu et al., 2020; Li et al., 2008; Liu et al. 2018; Yin et al., 2019), and have assessed the intensity and frequency of extreme rainfall events at the regional, national and global scales (Alexander et al., 2007; Almagro et al., 2017; Evans et al., 2016; Nearing et al., 2004). However, there have been few studies of rainfall erosivity during extreme events itself (Diodato et al., 2016; Wang et al., 2022). The long-term average value cannot fully represent the severity of the soil erosion process, and a few severe soil erosion events can contribute a great deal to the total amount of soil lost over many years (Bezak et al. 2021; Borrelli et al., 2016; Meusburger

et al., 2012; Petek et al., 2018). For example, field observations at the plot scale in eastern Austria showed that the three largest erosion events from 1994 to 2019 accounted for 79% of the total soil loss over the same period (Klik and Rosner, 2020). Zhou et al. (1992) reported that high-intensity, short-duration heavy precipitation events accounted for about 90% of the total annual soil erosion in the Loess Plateau region.

Extreme rainfall, which varies a great deal in space and time, can lead to severe flooding, with far-reaching implications for socio-economic and human activities (Fishman, 2016). With global warming, the frequency and intensity of extreme precipitation events are increasing mostly in mid-latitudes (Fang et al., 2017; IPCC 2021; Liao et al., 2019; Liu et al., 2017). Extreme rainfall, especially rainfall events with high intensity, is often more erosive (Fang et al., 2018; Huang et al., 2016a, 2016b, 2016c). Many studies reported that satellite-based products tended to underestimate the extreme rainfall, which can have an important effect on the estimation of rainfall erosivity using satellite-based products (Jiang et al., 2019; Palharini et al., 2020; Rahmawati and Lubczynski., 2018). For example, Bezak et al. (2022) showed CMORPH estimates had a marked tendency to underestimate rainfall erosivity in highly erosive areas when compared to the the GloREDa estimates. In addition, underestimation of extreme rainfall from climate models will lead to conservative projections of erosivity in highly erosive areas in the future (Panagos et al., 2022). Therefore, it is of great interest to examine the magnitude and frequency of occurrence of rainfall and rainfall erosivity of extreme storm events.

An extraordinarily heavy rainfall event occurred between 17th and 22th of July 2021 in Henan province. Such a rare event was never experienced or recorded in recent times in China. Record daily rainfall was observed at 10 meteorological stations in Zhengzhou, Xinxiang, Kaifeng, Zhoukou, Luoyang and other cities in Henan province. Zhang et al. (2021) reported that the storm was influenced by several weather systems including the eastward extension of the South Asian high, the abnormal northerly subtropical high, the Bengal Bay Depression at low latitude, the typhoon "Chapaca" in the South China Sea and the typhoon "Fireworks" in the Western Pacific. The strengthened and eastward extension of the South Asia high leads to an obvious divergence area of the upper atmosphere over Henan province, which is conducive to the upward movement of the lower atmosphere. The subtropical high, which is northward moving and stronger than usual for the same period, the No. 6 typhoon "Fireworks" and the No. 7 typhoon "Chapaca" in low latitudes, and the low pressure in Bengal Bay have led to the stable and lasting transmission of warm and humid airflow to Henan province (Zhang et al., 2021; Qian et al., 2022). Taihang Mountains and Funiu Mountains in the northwestern and western Henan province blocked the airflow, and a strong convergence formed in front of mountains, resulting in this extreme rainfall event.

The maximum hourly rainfall between 16:00 and 17:00 on 20 July reached 201.9 mm at Zhengzhou meteorological station, the highest ever recorded in China (Zhang et al., 2021). It has been widely reported that this extreme storm caused extensive flooding and landslides with damages to infrastructure and loss of human lives (Jin et al., 2022; Zhang et al., 2022). Event total rainfall, daily and hourly rainfall of the "7.20" storm have been reported elsewhere (Zhang et al. 2021), whereas rainfall erosivity associated with this extreme storm has not. The "7.20" storm presents a rare opportunity to examine the extreme rainfall erosivity in China. For this study, hourly rainfall data were used to evaluate the maximum daily and event rainfall erosivity, to estimate its average recurrence interval, to contextualize geographically the extreme erosivity of the "7.20" storm, to demonstrate how extreme the erosivity value of the "7.20" storm was and how large event rainfall erosivity could be in China, and to highlight the need to pay attention to extreme storm events and the huge erosion risk associated with them in the future.

2 Material and Methods

2.1 Data source and pre-processing

Observed hourly rainfall data from 1951 to 2021 for 2420 meteorological stations in China were collected by siphon rain

gauges or tipping bucket rain gauges. The instrument used by China Meteorological Administration (CMA) is SL3-1 tipping bucket rain sensors, and precipitation was measured according to the operation manual to meet certain standards at all stations. Tipping bucket rain gauges have a rainfall bearing diameter of 200 mm, and its resolution is 0.1 mm. The maximum allowable rainfall intensity is 4 mm·min^{-1}, and the maximum allowable rainfall error is ± 4 mm for every 100 mm. The rainfall data acquired from ~~China Meteorological Administration (CMA)~~ CMA and the data had been quality-controlled by CMA's National Meteorological Information Center. However, we found some unexpected errors in the data, so we checked hourly with daily observation from rain gauges. Hourly observations in early days were mainly digitized from precipitation autographic charts on paper. From 2000 to 2005, automatic weather stations were put into use and their introduction was gradually accelerated. Since 2005, nearly all observations were recorded with automatic weather stations. Hourly rainfall data from 796 meteorological stations in Henan and its surrounding nine provinces (municipalities) from 20:00 (Beijing time) on 16 July and to 20:00 on 22 July 2021 were used to characterize the "7.20" storm. Hourly rainfall data from 1951 to 2020 were used to calculate the annual maximum daily and event rainfall erosivity. To reduce the impact of missing values on the result, years with missing data were discarded. A year with missing data was defined as follows: if there were four or more hours of missing records on a given day, it was considered as a missing day and if the number of missing days in a month ≥ six, it was considered as a missing month. Since most of the rainfall in the north of China (north of 32°N) is concentrated from May to September, the year with any month from May to September missing was defined as a missing year. In southern China (south of 32°N), the year with any month from April to October missing is defined as a missing year. Missing years were removed, and missing values in effective years are input as zero value.

Figure 1. Spatial distribution of stations with hourly rainfall data and the record length.

2.2 Framework of study

2.2.1 Definition of rainfall events and rainfall parameters

An event was defined as a period of rainfall separated with dry periods greater than "minimum inter-event time" (MIT). The MIT in the USLE and RUSLE2 ~~was~~ is six hours. In this study, MIT of six hours was used to define rainfall events. The maximum event rainfall, maximum daily rainfall, maximum hourly rainfall and maximum event rainfall erosivity were computed following to the framework shown in Fig. 2. Since there were multiple events over the six-day in period during the "7.20" storm, the maximum event rainfall was the maximum rainfall amount of all events over the six-days period. Maximum event rainfall erosivity was similarly defined.

2.2.2 Calculation of the energy and daily/event rainfall erosivity

Hourly data were used to calculate the rainfall erosivity, EI_{30} (MJ·mm·ha^{-1}·h^{-1})for each event, which is the product of the event energy and peak 30-min intensity. All the hourly data for day (8:00 pm to 8:00 pm) were used to compute daily rainfall erosivity. Rainfall kinetic energy is used by most erosion models for assessing the capacity of rainfall to produce erosion. Rainfall kinetic energy is a function of raindrop size and falling velocity. Because the direct measurement of kinetic energy (KE) requires complex and expensive instruments, many different estimation methods have been developed. These methods use logarithmic, exponential, or power law formulas to derive kinetic energy-intensity (KE-I) relationships. The most widely accepted kinetic energy-intensity relationship is the exponential model proposed by Kinnell (1981). The rainfall kinetic energy is calculated by

Eq. (2), which includes the modification suggested by McGregor et al. (1995). The total energy (EN, MJ·ha^{-1}) of an erosive event was computed using following equations (USDA-ARS, 2013):

$$EN = \sum_{r=1}^{l}(e_r \cdot P_r) \tag{1}$$

$$e_r = 0.29 \cdot [1 - 0.72 \cdot exp(-0.082 \cdot i_r)] \tag{2}$$

where a rainfall event ~~was~~ is divided into l periods, each with an intensity, i_r (mm·h^{-1}), P_r (mm) ~~was~~ is the rainfall amount for the rth period and e_r (MJ·mm^{-1}·ha^{-1}) ~~was~~ is the energy per unit rainfall per unit area for the rth period. The event rainfall erosivity can be estimated with of EN and I_{1h} (USDA-ARS, 2013):

$$EI_{1h} = EN \cdot I_{1h} \tag{3}$$

$$EI_{30} = 1.489 \cdot EI_{1h} \tag{4}$$

where I_{1h} ~~was~~ is the peak one-hour rainfall intensity for the erosive event, and the conversion factor of 1.489 was used to correct the bias in the rainfall erosivity using hourly rainfall data, and the standard error of the conversion factor is ± 0.064 (Yue et al., 2020).

Total rainfall and energy over the six days of the "7.20" storm for 796 stations were interpolated ~~into grid data with~~ spatially at 100 m spatial resolution, and the regional averages ~~of~~ for Henan province and the study area (Henan province and its surrounding nine provinces/municipalities) were calculated and compared with Zhengzhou meteorological station.

~~We used inverse distance weighting (IDW) to interpolate point data to map rainfall erosivity distribution for the region.~~ The rainfall and rainfall erosivity maps were generated by the interpolation of rainfall and rainfall erosivity values from at-site rainfall observations by geostatistics techniques, such as the inverse distance weighting, or ordinal Kriging (Panagos et al., 2015; Sadeghi et al., 2017; Yin et al., 2019). We used inverse distance weighting (IDW) to interpolate point data to map rainfall and rainfall erosivity distribution for the region. The IDW method computes precipitation at the interpolating point by assigning larger weights to observation stations closer to the target grid (Shepard, 1968).

2.2.3 Log Pearson type III distribution

An annual series is defined here as a collection of maxima, one from each calendar year. Annual series of the maximum daily and event rainfall erosivity from the period 1951-2020 ($n = 67$ due to three missing years) for Zhengzhou meteorological station were sorted in a descending order with the largest assigned a rank of one. The empirical return period, or the average recurrence interval, of each observation in the annual series was calculated according to the following formula (Bobeé and Robitaille, 1977):

$$RP = \frac{n+1}{m} \tag{5}$$

where RP is the empirical return period in years, n ~~was~~ is the number of years or the sample size, and m ~~was~~ is the rank ($m = 1$ for the largest).

The probability distribution used to fit the annual series was the log Pearson type III (LP-–III) distribution. LP-–III distribution is considered a suitable model for flood frequency estimation in many investigations (Bobeé and Robitaille, 1977; England et al., 2003; England, 2019). The logarithms of the annual series of the maximum daily rainfall erosivity and the maximum event rainfall erosivity from 1951-2020 for Zhengzhou meteorological station were used to fit the Pearson type III distribution (P-III), respectively. The probability density function (PDF) and cumulative distribution function (CDF) of P-III distribution model are as follows:

$$f(x) = \frac{\beta^\alpha}{\Gamma(\alpha)}(x - a_0)^{\alpha-1}e^{-\beta(x-a_0)} \quad x > a_0, \alpha > 0, \beta > 0 \tag{6}$$

$$F(x) = \frac{\beta^\alpha}{\Gamma(\alpha)}\int_{a_0}^{x}(x - a_0)^{\alpha-1}e^{-\beta(x-a_0)}dx \tag{7}$$

where x is the random variable of interest, a_0 ~~was~~ is the location parameter, α the shape parameter, and β the scale parameter. $\Gamma(\alpha)$ is the gamma function. The basic parameters, mean $\bar{x}$, coefficient of variation C_V, and skewness coefficient

C_S, were used to estimate parameter a_0, α and β (Viessman Jr. and Lewis, 2002) (Eq. 8-10), and the 95% confidence interval was also estimated (Kite, 1975).

$$\alpha = \frac{4}{C_S} \tag{8}$$

$$\beta = \frac{2}{\bar{x} C_S C_v} \tag{9}$$

160
$$a_0 = \bar{x}(1 - \frac{2C_v}{C_S}) \tag{10}$$
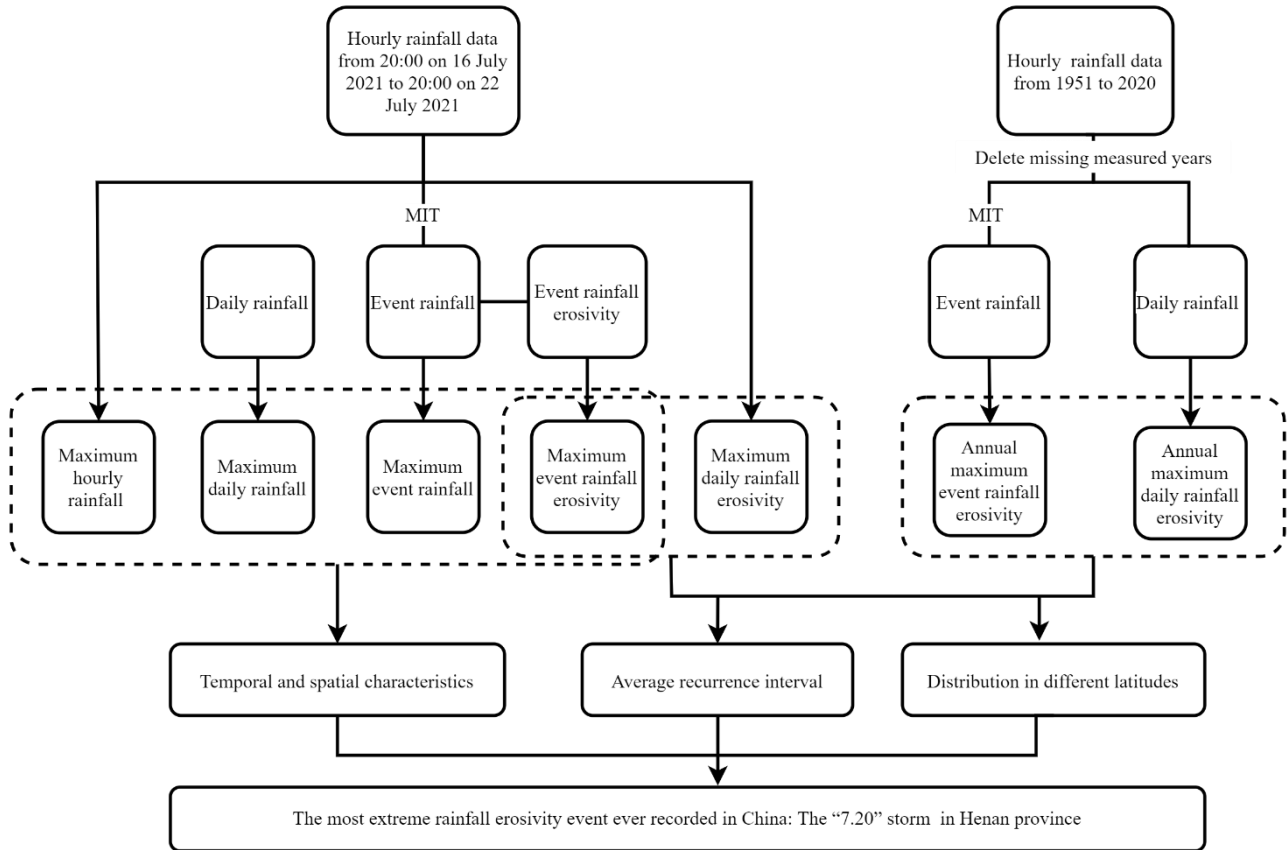
Figure 2. Framework for this study

3 Results and discussion

3.1 Temporal and spatial characteristics of the "7.20" storm

165 *3.1.1 Characteristics of the "7.20" storm*

The extreme event occurred in Henan province between 20:00 on 16 July 2021 and 20:00 on 22 July 2021. The center of the storm center is mainly located around Zhengzhou. The storm duration was long and accumulated rainfall was huge. Spatial pattern of accumulated rainfall of the "7.20" storm is shown in Fig. 3a. The top three rainfall stations were Zhengzhou (817.3 mm), Huixian (755.2 mm) and Xinmi (723.5 mm). Additionally, among the 797 automatic meteorological stations in the study

170 area, 58 meteorological stations have accumulated rainfall of more than 250 mm, of which 50 are located in Henan province. Rainfall mass curves for these three stations are shown in Fig. 3b. Obviously, the rainstorm at Zhengzhou meteorological station and Xinmi station contributed more than 50 % of the rainfall in the middle period, while the rainstorm at Huixian station contributed more than 50 % of the rainfall in the last period. Wang et al. (2016) have demonstrated that different rainstorm patterns with rainfall peak in the early, middle and late stages have different effects on soil erosion process, under the natural

175 rainfall conditions. n that study, storms were classified into four patterns: the advanced, intermediate, delayed, and uniform depending when rainfall is most concentrated. The dimensionless durations were separated into three equal periods. Advanced pattern, intermediate pattern and delayed pattern when more than 40 % of the rainfall occurs in the first, second and third periods, respectively. The rainfall temporal distribution is regarded as the uniform pattern otherwise. Wang's research showed that given the same EI30, the rainstorm pattern with rainfall peak at the later stage produced more soil loss than the other

180 patterns (Wang et al., 2016).
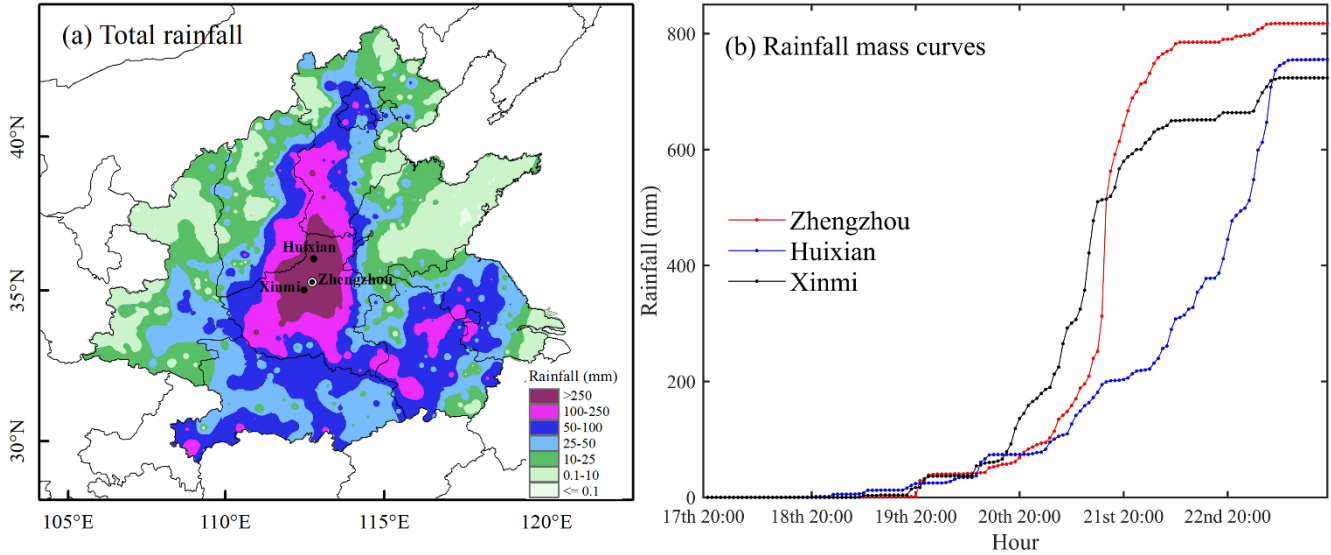
Figure 3. ~~Distribution~~ A map of total rainfall over the study area, and rainfall mass curves for three stations with the largest rainfall totals.

Spatial pattern of daily rainfall of the "7.20" storm in the study area is shown in Fig. 4. Heavy rainfall mainly occured in the middle and late stages of the event. The maximum daily rainfall (Zhengzhou, 552.5 mm) occurred on 20 July (Fig.

185 4d), while the storm was most extensive on 21 July (Fig. 4e). The storm is initially concentrated in the Anhui provinces (Fig. 4a), and then dispersed somewhat on 18 July (Fig. 4b). On 19 July, the storm re-appears in the central region of Henan province (Fig. 4c). On 20 July, the storm began to intensify and expand its spatial extent (Fig. 4d). The daily rainfall at 39 meteorological stations exceeded 100 mm, and the daily rainfall of seven meteorological stations exceeded 250 mm on 20 July. On 21 July (Fig. 4e), the center of the storm began to move northward, and the rainfall intensity started to dissipate, and

190 the storm now covered a large area with storm center drifted north to Tangyin (388.2 mm), Henan province, and recorded rainfall at 48 meteorological stations exceeded 100 mm and six meteorological stations exceeded 250 mm. The rainfall decreased considerably by 22 July (Fig. 4f). The storm center was located in the north of Henan province, and the rainfall at 16 meteorological stations exceeded 100 mm.
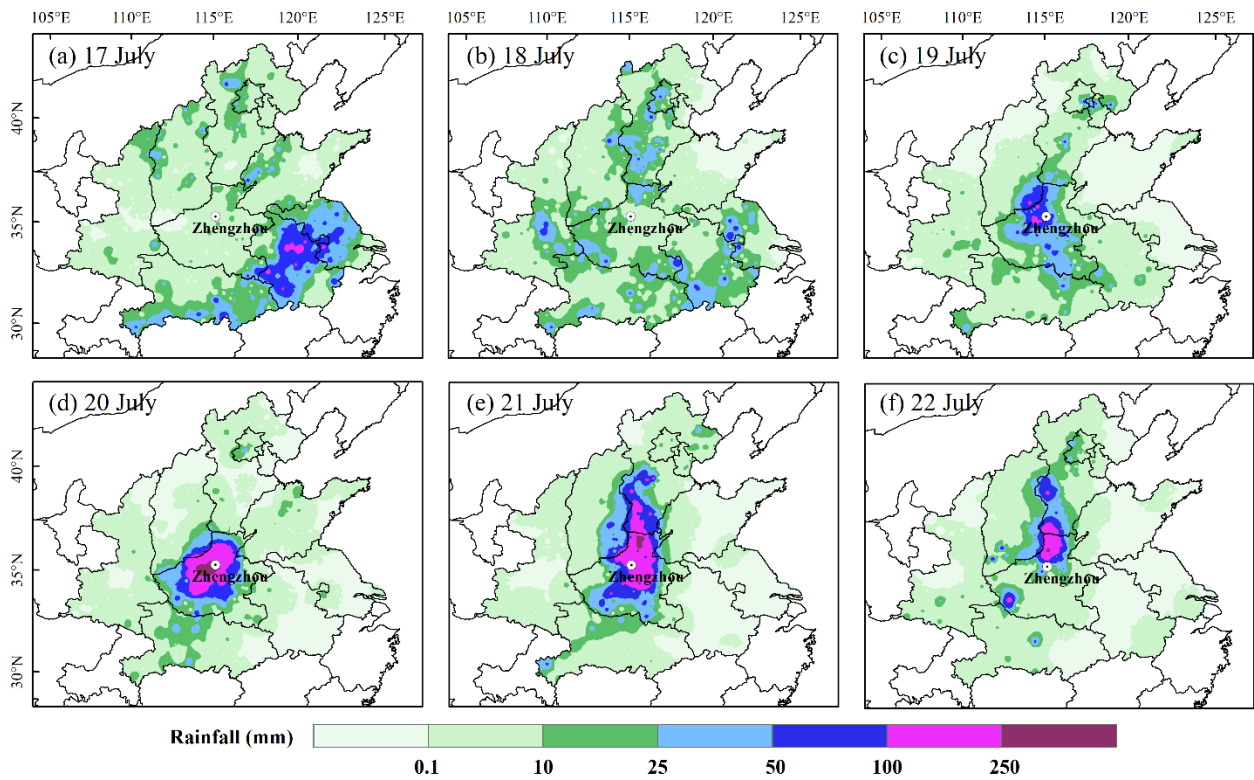
Figure 4. Spatial ~~pattern~~ distribution of daily rainfall in the study area. Daily rainfall is rainfall accumulation over 24-hour period, e.g. daily rainfall on 20 July is the total rainfall from 20:00 on 19 July to 20:00 on 20 July.

3.1.2 The spatial distribution of rainfall parameters and rainfall erosivity

The spatial distribution of maximum daily and hourly rainfall amount, and maximum event rainfall and rainfall erosivity are shown in Fig. 5. At the center of the storm, a maximum event rainfall amount of 785.1 mm and a maximum daily rainfall amount of 552.5 mm on 20 July were recorded at Zhengzhou meteorological station. From 16:00 to 17:00 on 20 July, maximum hourly rainfall reached 201.9 mm at Zhengzhou meteorological station, and created a new hourly rainfall intensity record (201.9 mm·h^{-1}) in mainland China. The maximum event rainfall erosivity in the area with Zhengzhou meteorological station has reached 58,874 MJ·mm·ha^{-1}·h^{-1}. Due to the uncertainty with the conversion factor, the maximum rainfall erosivity could range from 56,343 MJ·mm·ha^{-1}·h^{-1} to 61,404 MJ·mm·ha^{-1}·h^{-1}.
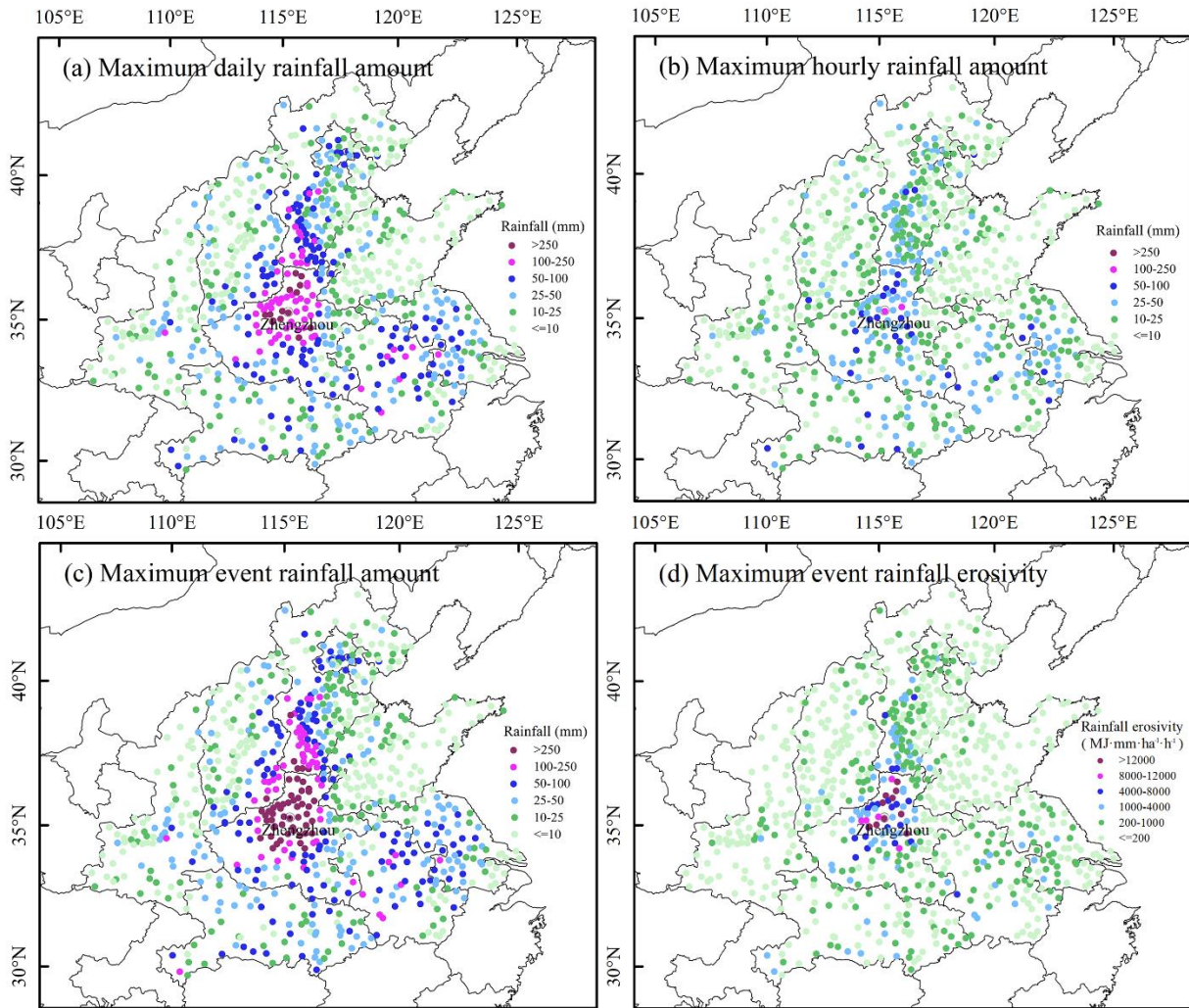
Figure 5. Spatial distribution of rainfall amount and rainfall erosivity associated with the "7.20" storm.

3.1.3 Rainfall's total kinetic energy

Table 1. The composition of average rainfall and energy in different regions from 20:00 on 16 July 2021 to 20:00 on 22 July 2021

Region	Index	17th	18th	19th	20th	21st	22nd	Total
Study area (1.33×10⁸ ha)	Mean rainfall (mm)	12.4	10.0	6.8	8.7	11.3	5.8	55.0
	EN (MJ·ha⁻¹)	2.6	2.0	1.3	1.7	2.3	1.1	11.0
Henan province (1.66×10⁷ ha)	Average rainfall (mm)	5.8	13.5	26.6	70.5	61.9	21.5	199.8
	EN (MJ·ha⁻¹)	2.0	3.0	4.8	13.5	15.6	7.1	46.0
Zhengzhou meteorological station	Average rainfall (mm)	0.0	1.3	60.2	552.5	176.0	27.3	817.3
	EN(MJ·ha⁻¹)	0.0	0.1	12.3	144.2	40.0	4.0	200.6

The detachment of soil particles from the soil mass and the transportation of detached particles by raindrop impact and surface water flow are two main processes of soil erosion. Rainfall energy reflects the impact of raindrop detachment on the soil. The average rainfall and energy for each meteorological day over different regions of "7.20" storm were listed in Table. 1. Comparing the three regions, the average rainfall and EN in the study area on 17 July are higher than those in Henan province and Zhengzhou meteorological station, indicating that the rainstorm center may be outside Henan province at this time. With the movement of rainstorm center, the average rainfall and EN of Henan province and Zhengzhou meteorological station gradually increase. The average rainfall in Henan province reached its peak on 20 July (70.5 mm), but EN reached its peak on 21 July (15.6 MJ·ha⁻¹). The average rainfall and EN of Zhengzhou meteorological station reached the peak on 20 July, which

were 552.5 mm and 144.2 MJ·ha^{-1} respectively. The energy of Zhengzhou meteorological station on 20 July is 11 times of average energy in Henan province.

In summary, an extraordinarily heavy rainfall event occurred in Henan province between 20:00 on 16 July 2021 and 20:00 on 22 July 2021. Among them, the observations of Zhengzhou Meteorological Station show that the maximum event rainfall is 785.1 mm, the maximum daily rainfall is 552.5 mm, the maximum hourly rainfall intensity is 201.9 mm·h^{-1} and the maximum event rainfall erosivity is 58,874 MJ·mm·ha^{-1}·h^{-1}. The storm is initially concentrated in the southeast of Henan and Anhui provinces, and the rainfall and rainfall intensity reached the peak on 20 July. At the same time, the rainstorm center moved to the north of Henan province with Zhengzhou as the center of the rainstorm. The EN of Zhengzhou Meteorological Station reached 144.2 MJ·ha^{-1} on 20 July. It can be seen that the "7.20" storm has the characteristics of long duration, heavy cumulative rainfall, a wide range of heavy rainfall, and extremely strong short-term rainfall. It is a particularly serious natural disaster that caused serious urban waterlogging, mountain floods, landslides and other disasters, resulting in heavy casualties and serious economic losses.

3.2 How extreme is the event recorded at Zhengzhou meteorological station?

3.2.1 Frequency of occurrence the maximum daily and event rainfall erosivity

Annual maximum daily rainfall erosivity and the annual maximum event rainfall erosivity in Zhengzhou meteorological station from 1951 to 2020 are shown in Fig. 6 along with fitted LP-III distribution. Three frequency distributions were considered and tested, including Generalized extreme value (GEV), P-III, and P-III, and LP-III was found to be the most appropriate (Table. S2, supplementary material). All the three distributions fitted the observations well, and performance indicator values do not suggest a single distribution that consistently and significantly superior to others. Given LP-III was widely recommended for extreme precipitation and flood events in China (Chen et al., 2012), LP-III was used to assess the return period of this "7.20" storm. It can be seen from Fig. 6 & 7 that the LP-III distribution fits the maximum daily rainfall erosivity and the maximum event rainfall erosivity well. Using the fitted LP-III distribution, the average recurrence interval of the maximum daily rainfall erosivity of the "7.20" storm is estimated to be about 23,100 years with the lower and upper limits of the 95% confidence intervals are [8200, 228,000] years, and the ratio of the observed daily erosivity (43,354 MJ·mm·ha^{-1}·h^{-1}) over 1-in-100-year daily erosivity (7551 MJ·mm·ha^{-1}·h^{-1}) is 5.74. Similarly, the average recurrence interval of the maximum event rainfall erosivity is estimated to be about 10,000 years with the lower and upper limits of the 95% confidence intervals are [9400, 367,000] years, the observed event erosivity of the "7.20" rainstorm (58,874 MJ·mm·ha^{-1}·h^{-1}) is 6.17 times larger than the 1-in-100-year event erosivity (9544 MJ·mm·ha^{-1}·h^{-1}). Based on the 95% confidence interval for the LP-III distribution, the estimated return period of the maximum daily and event rainfall erosivity is most likely to be at least 785 and 516 years. Evidently, compared with observations in the past decades (1951-2020), the maximum daily and event rainfall erosivity of the "7.20" storm in 2021 is extraordinary, and the event is so rare and extreme that it should be regarded as an outlier among observations in other years.
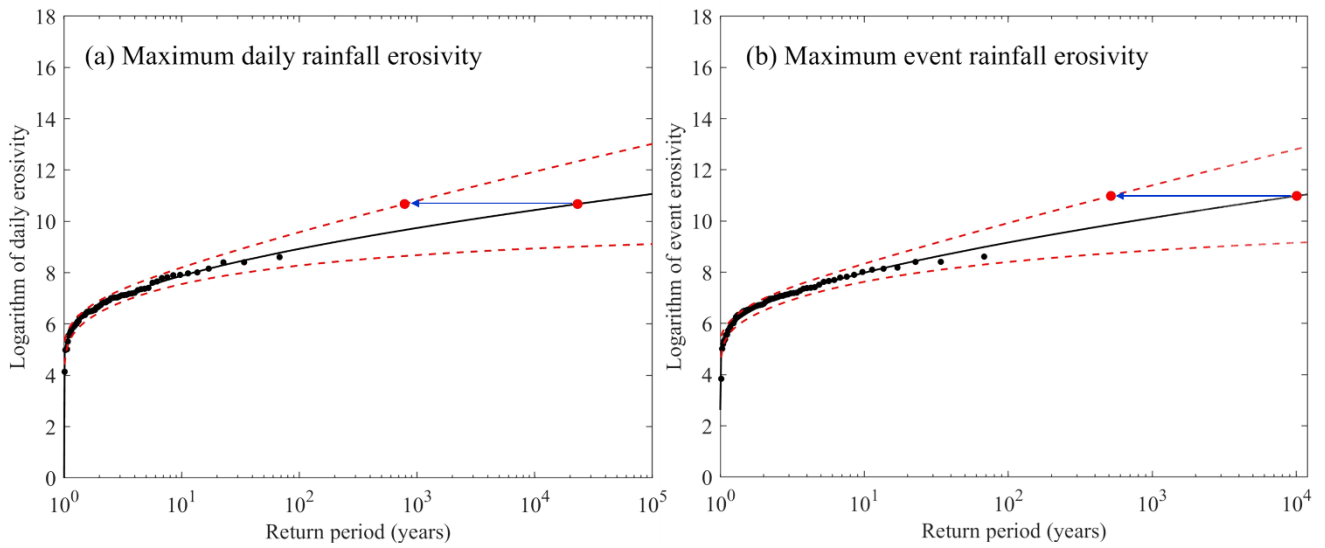
250 **Figure 6.** The logarithm of observed daily (a) and event (b) rainfall erosivity as a function of the ~~empirically fitted~~ return period assuming LP-III for at Zhengzhou meteorological station. Black solid circles are observations from the period 1951-2020, the red solid circles indicate the "7.20" storm in 2021, the red dotted line is the upper and lower limit of 95% confidence interval, and the solid lines in black represent the fitted P-III distribution using the logarithm of observations from 1951-2020.
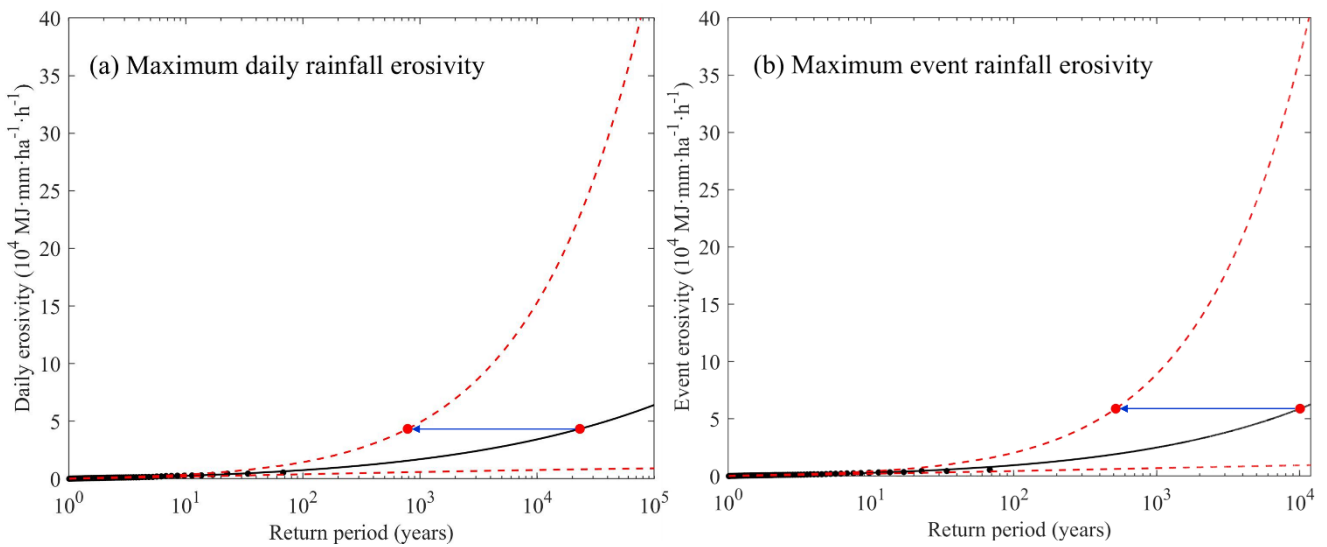
255 Figure 7. Observed daily (a) and event (b) rainfall erosivity as a function of the ~~empirically fitted~~ return period assuming LP-III for Zhengzhou meteorological station (Performed anti-logarithm conversion for Fig. 6)

The map of the return period of maximum daily and event rainfall erosivity of the "7.20" storm in Henan province is shown in Fig. 8. Similar to Zhengzhou meteorological station, ~~, by fitting the LP-III distribution,~~ the map of the return period of rainfall erosivity of "7.20" storm in the study area was drawn by fitting the LP-III distribution. The map shows that the 260 return periods of daily (11 stations) and rainfall (16 stations) erosivity at some meteorological stations exceed 1-in-100-year, mainly in the northern region of Henan province, with Zhengzhou meteorological station as the center of the "7.20" storm.
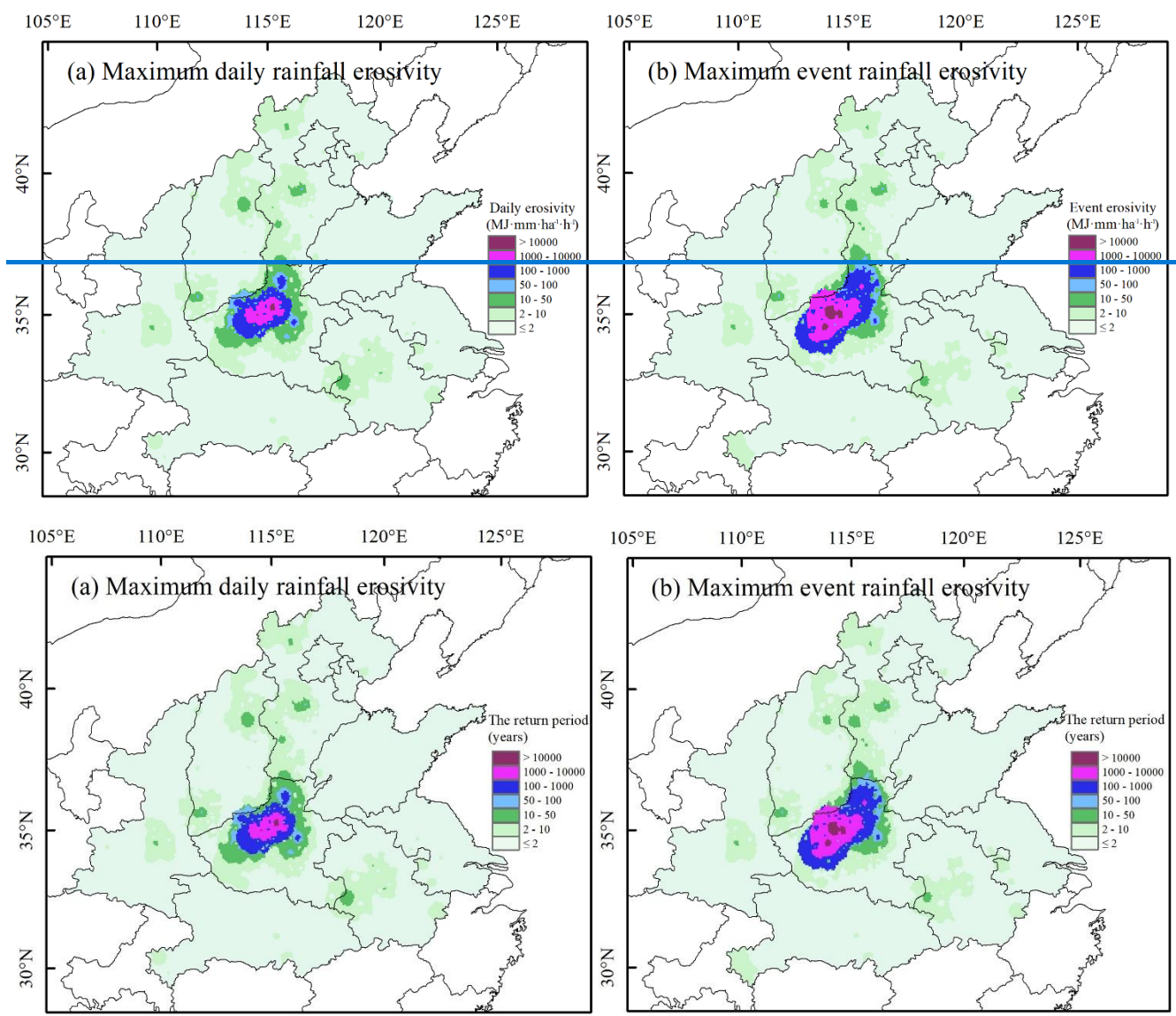
Figure 8. The return period of daily (a) and event (b) rainfall erosivity of the "7.20" storm in the study area.

3.2.2 Distribution of the maximum rainfall erosivity in different latitudes

Geographical distribution of the maximum daily rainfall erosivity ever recorded at each of 2420 meteorological stations in China is shown as a function of the latitude in Fig. 9. Envelope curves I and II are drawn for the scatter plot, and the stations and the corresponding daily rainfall and rainfall erosivity values that were used to define these envelope curves are given in Table. 2. The two envelope curves overlap at three stations at low latitude and one at high latitude, and the change from curve I to II in the middle latitude is entirely a result of the "7.20" storm in 2021. Prior to the "7.20" storm, curve I shows that the maximum recorded daily rainfall erosivity decreases from about 20°N as the latitude increases, and the maximum daily erosivity value was 39,345 MJ·mm·ha^{-1}·h^{-1}, recorded Maoming meteorological station in Guangdong province (21.75°N) on 5 June 2020. Because of the "7.20" rainstorm, the maximum daily rainfall erosivity ever recorded was increased to 43,354 MJ·mm·ha^{-1}·h^{-1} or by more than 10 % at Zhengzhou meteorological station (34.72°N) on 20 July 2021.
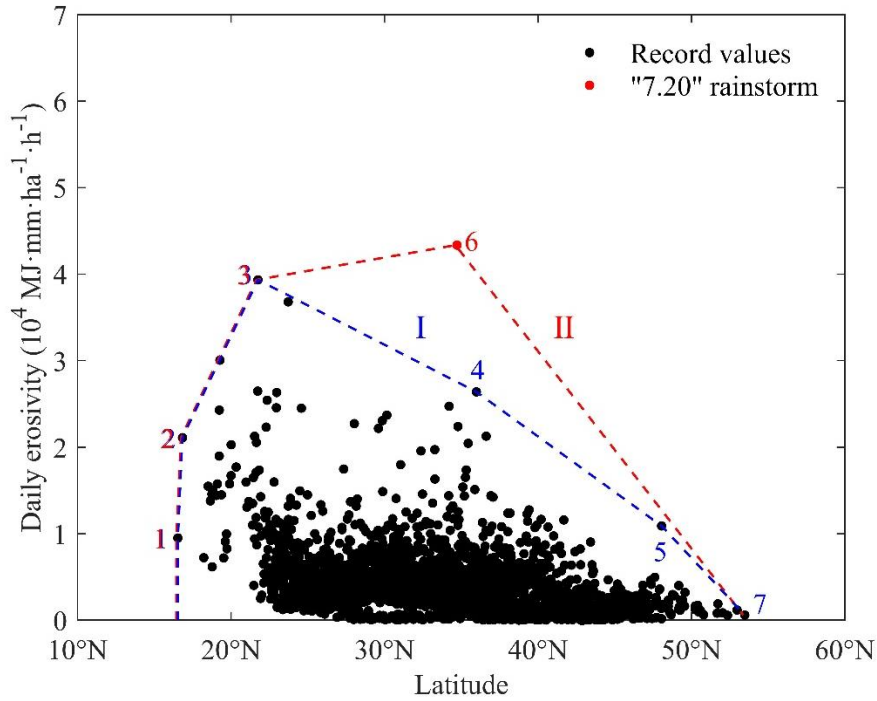
Figure 9. The maximum recorded daily rainfall erosivity as a function of latitude for China. The point enclosed by the envelope curve I is the maximum daily rainfall erosivity of each station from 1951 to 2020. The point enclosed by envelope curve II is the maximum daily rainfall erosivity of each station from 1951 to 2021.

Table 2. The mean annual rainfall, maximum daily rainfall and rainfall erosivity for stations to define envelope curves.

| ID | | Station ID | Station name | Latitude | Mean annual rainfall (mm) | Daily rainfall (mm) | Daily rainfall erosivity (MJ·mm·ha^{-1}·h^{-1}) | Date |
I	II							
1	1	59985	Shanhu	16.53	1316.0	227.6	9512	1980-09-12
2	2	59981	Xisha	16.83	1467.9	585.6	21104	1995-09-05
3	3	59659	Maoming	21.75	1701.7	307.3	39345	2020-06-05
4		54848	Zhucheng	35.98	623.8	592	26398	1999-08-12
5		50658	Keshan	48.05	445.4	179.6	10909	1957-07-15
	6	57083	Zhengzhou	34.72	566.7	552.5	43354	2021-07-20
7	7	50137	Beijicun	53.47	385.2	77.6	603	2010-07-31

Geographical distribution of the maximum event rainfall erosivity ever recorded at each of 2420 meteorological stations in China is shown as a function of the latitude in Fig. 10. Envelope curves I and II are drawn for the scatter plot, and the stations and the corresponding event rainfall and rainfall erosivity values that were used to define these envelope curves are given in Table. 3. The two envelope curves overlap at three stations at low latitude and one at high latitude, and the change from curve I to II in the middle latitude is entirely a result of the extreme "7.20" storm in 2021. Prior to the "7.20" storm, curve I shows that the maximum recorded event rainfall erosivity decreases from about 20°N as the latitude increases, and the maximum ever event erosivity value was 41,537 MJ·mm·ha^{-1}·h^{-1}, recorded Maoming meteorological station in Guangdong province (21.75°N) from 20:00 on 20 May 1987 to 18:00 on 22 May 1987. Because of the "7.20" storm, the maximum event rainfall erosivity ever recorded was increased to 58,874 MJ·mm·ha^{-1}·h^{-1}, or an increase of more than 40 % at Zhengzhou meteorological station (34.72°N) on 20 July 2021.
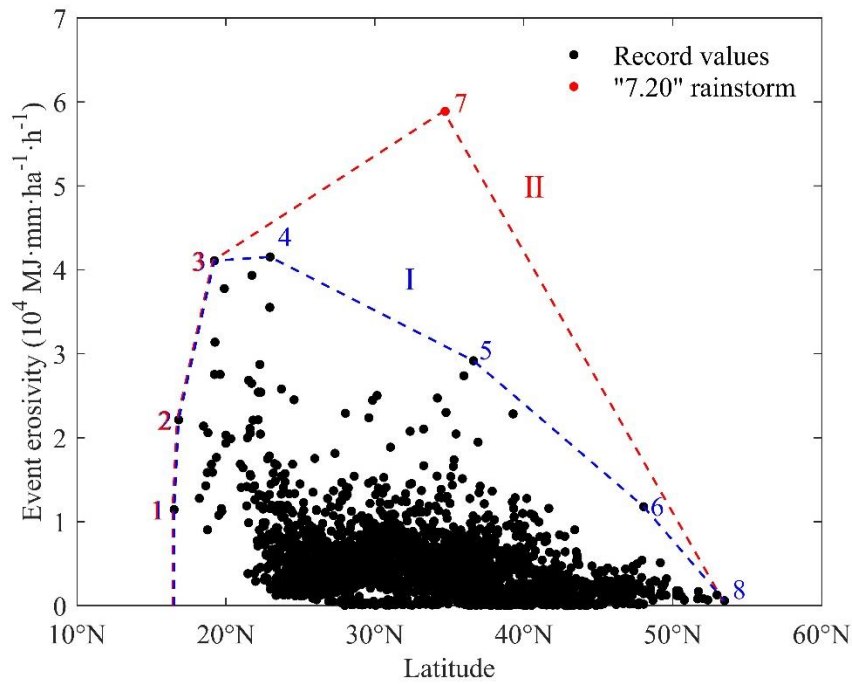
Figure 10. The maximum recorded event rainfall erosivity as a function of latitude for China. The point enclosed by the envelope curve I is the maximum event rainfall erosivity of each station from 1951 to 2020. The point enclosed by envelope curve II is the maximum event rainfall erosivity of each station from 1951 to 2021.

Table 3. The mean annual rainfall, maximum event rainfall and rainfall erosivity for stations to define envelope curves.

ID		Station ID	Station name	Latitude	Starting date and time	End date and time	Mean annual rainfall (mm)	Event rainfall (mm)	Event rainfall erosivity (MJ·mm·ha^{-1}·h^{-1})
I	II								
1	1	59985	Shanhu	16.53	1980-09-11 11:00	1980-09-12 8:00	1316.0	288.2	11446
2	2	59981	Xisha	16.83	1995-09-05 8:00	1995-09-06 23:00	1467.9	625.5	22135
3	3	59855	Qionghai	19.23	2010-10-01 22:00	2010-10-08 15:00	2021.7	1433.3	41083
4		59500	Haifeng	22.97	1987-05-20 20:00	1987-05-22 18:00	2407.5	987.3	41537
5		53892	Handan	36.62	1963-08-03 3:00	1963-08-06 1:00	478.8	748.1	29174
6		50658	Keshan	48.05	1957-07-15 14:00	1957-07-15 24:00	445.4	199.5	11794
	7	57083	Zheng-zhou	34.72	2021-07-18 8:00	2021-07-21 10:00	566.7	785.1	58874
8	8	50137	Beijicun	53.47	2010-07-30 23:00	2010-07-31 14:00	385.2	77.6	603

295   A large number of studies have shown that the mean annual rainfall and rainfall erosivity, i.e. the R-factor, decrease from southeast to northwest in China (Yin et al., 2019; Yue et al., 2022), that is, the mean annual rainfall and rainfall erosivity is the highest at low latitude in China. Like rainfall, the average rainfall intensity for given storm duration also tends to be high at low latitude, and low at high latitude in China (Kong et al., 2017). Thus, one would expect that maximum daily and event rainfall erosivity tends to decrease with the latitude, a trend largely supported by the envelope curve I in Fig. 9 & 10. The

300   "7.20" storm may have fundamentally changed the nature and distribution of extreme daily and event erosivity in China as we knew them up to now. This is consistent with the research of Wang and Luo (2006), and the storm extreme value does not always conform to the pattern of decreasing from low latitude to high latitude. For example, based on measured and surveyed rainfall records, the maximum 24-hour rainfall depth occurred at Linzhuang in Henan province in the mid-latitude on 5–7 August 1975 (Ding., 2015). Occurrence of this "7.20" storm in 2021 around Zhengzhou has important implications. First,

Figure. 9 & 10 suggest that extreme event erosivity may be the highest in mid-latitude around 35°N despite the fact the mean annual rainfall and rainfall intensity are by no means the highest in mid-latitude in China. Second, the "7.20" storm was ~~so rare and freakish~~out of ordinary that the event was seemingly unrelated to the underlying climatology. Finally, the "7.20" storm has led us to realize that such extreme erosive events could and may occur anywhere in eastern China with further implications for soil conservation planning.

4 Conclusions

This study assessed an extreme rainfall event in Henan province from 20:00 on 16 July 2021 to 20:00 on 22 July 2021, using hourly rainfall data from 796 stations in Henan and surrounding provinces. Based on hourly rainfall data of 2420 meteorological stations in China from 1951 to 2021, the annual maximum daily and event rainfall erosivity of Zhengzhou meteorological station were fitted with the LP-III distribution to evaluate magnitude and frequency of occurrence of this extreme event in terms of rainfall amount and erosivity values. The following conclusions can be drawn ~~as follows~~as a result of this research:

(1) The maximum event rainfall (785.1 mm), maximum daily rainfall (552.5 mm), maximum hourly rainfall intensity (201.9 mm·h^{-1}) and maximum event rainfall erosivity (58,874 MJ·mm·ha^{-1}·h^{-1}) of "7·20" storm all occurred and were recorded at Zhengzhou meteorological station. The period of the highest rainfall intensity was mainly concentrated in the middle and late stages of the storm, reaching its peak on 20 July, producing a daily total of 144.2 MJ·ha^{-1} energy.

(2) Based on long-term observations for the period 1951-2020 and the fitted LP-III distribution, the "7.20" storm was estimated to have an average recurrence interval in excess of 10,000 years, and the annual maximum daily and event rainfall erosivity were about six times larger than 1-in-100-year erosivity values.

(3) This extreme event recorded at the Zhengzhou meteorological station has set a new record for daily and event rainfall erosivity values in mainland China. The "7.20" rainstorm in 2021 was ~~so~~ extremely rare ~~and freakish~~, and suggested to us that extreme erosive events could and may occur anywhere in eastern China, rather than in low latitude with high rainfall amount and rainfall intensity as we previously knew and expected.

~~Author~~ Data ~~contributions~~Availability. Observed hourly rainfall data from National Meteorological Information Center of the China Meteorological Administration (NMIC, http://data.cma.cn).

Author contributions. Y Xiao, S Yin and B Yu conceived and designed this study. Y Xiao undertook data analysis and interpretation, prepared all the diagrams, and drafted the manuscript. S Yin and B Yu guided data analysis and interpretation. All authors reviewed and edited the manuscript.

Competing interests. The authors declare that they have no conflict of interest.

Financial support. This research has been supported by the National Key Research and Development Program of China (grant no. 2021YFE0113800), National Natural Science Foundation of China (grant no. 41877068) and the project "ACRP 13: Soil erosion in Austria -from mean to extreme (EROS-A)" funded by the Klima- und Energiefonds.

References

345   Alexander, L.V., Hope, P., Collins, D., Trewin, B., Lynch, A., and Nicholls, N.: Trends in Australia's climate means and extremes: a global context, Aust. Met. Mag., 56, 1–18, 2007.

Almagro, A., Oliveira, T. P. S., Nearing, M. A., and Hagemann, S.: Projected climate change impacts in rainfall erosivity over Brazil, Sci. Rep., 7, 8130, https://doi.org/10.1038/s41598-017-08298-y, 2017.

Bobeé, B. B., and Robitaille, R.: The Use of the Pearson Type 3 and Log Pearson Type 3 Distributions Revisited, Water Resour.
350   Res., 13(2), 427–443, https://doi.org/10.1029/WR013i002p00427, 1977.

Borrelli, P., Diodato, N., and Panagos, P.: Rainfall erosivity in Italy: a national scale spatio-temporal assessment, Int. J. Digit. Earth., 9(9), 835–850. https://doi.org/10.1080/17538947.2016.1148203, 2016.

Bezak, N., Mikoš, M., Borrelli, P., Liakos, L., and Panagos, P.: An in-depth statistical analysis of the rainstorms erosivity in Europe, Catena, 206, 105577, https://doi.org/10.1016/j.catena.2021.105577, 2021.

355   Bezak, N., Borrelli, P., and Panagos, P.: Exploring the possible role of satellite-based rainfall data in estimating inter- and intra-annual global rainfall, Hydrol. Earth Syst. Sci., 26, 1907–1924, https://doi.org/10.5194/hess-26-1907-2022, 2022

Chen, L., Singh, V. P., Guo, S. L., Hao, Z. C., and Li, T. Y.: Flood coincidence risk analysis using multivariate copula functions, J. Hydrol. Eng., 17(6): 742–755, https://doi.org/10.1061/(ASCE)HE.1943-5584.0000504, 2012.

Diodato, N., Bellocchi, G., Romano, N., and Guadagno, F. M.: Modelling the rainfall erosivity of the Rhone Region
360   (Southeastern France) associated with climate variability and storminess, Adv. Meteorol., 2016, 7626505, https://doi.org/10.1155/2016/7626505, 2016.

Ding, Y. H.: On the study of the unprecedented heavy rainfall in Henan Province during 4-8 August 1975: Review and assessment, Acta Meteorol. Sin. (in Chinese), 73(3): 411–424, http://dx.chinadoi.cn/10.11676/qxxb2015.067, 2015.

England, J. F., Jr., Salas, J. D. and Jarrett, R. D.: Comparisons of two moments-based estimators that utilize historical and
365   paleoflood data for the log Pearson type III distribution, Water Resour. Res., 39(9), 1243, https://doi.org/10.1029/2002WR001791, 2003.

England, J. F., Jr., Cohn, T. A., Faber, B. A., Stedinger, J. R., Thomas, W. O., Jr., Veilleux, A. G., Kiang, J. E., and Mason, R.: Guidelines for Determining Flood Flow Frequency-Bulletin 17C, Techniques and Methods 4-B5, U.S. Geological Survey, Reston, VA, USA, 2019.

370   Evans, J.P., Arguesco, D., Olson, R., and Di Luca, A.: Bias-corrected regional climate projections of extreme rainfall in south-east Australia, Theor. Appl. Climatol., 130(3–4), 1085–1098, https://doi.org/10.1007/s00704-016-1949-9, 2016.

Fang, W., Huang, Q., Huang, S. Z., Yang, J., Meng, E. H., and Li, Y. Y.: Optimal sizing of utility-scale photovoltaic power generation complementarily operating with hydropower: a case study of the World's largest hydro-photovoltaic plant, Energy Convers. Manag., 136, 161–172, https://doi.org/10.1016/j.enconman.2017.01.012, 2017.

375   Fang, W., Huang, S.Z., Huang, Q., Huang, G. H., Meng, E. H., and Luan, J. K.: Reference evapotranspiration forecasting based on local meteorological and global climate information screened by partial mutual information, J. Hydrol., 561, 764–779, https://doi.org/10.1016/j.jhydrol.2018.04.038, 2018.

Fishman, R.: More uneven distributions overturn benefits of higher precipitation for crop yields, Environ. Res. Lett., 11(2), 024004, https://doi.org/10.1088/1748-9326/11/2/024004, 2016.

380   Gu, Z. J., Feng, D. T., Duan, X. W., Gong, K. F., Li, Y. W., and Yue, T. Y.: Spatial and Temporal Patterns of Rainfall Erosivity in the Tibetan Plateau, Water, 12(1), 200, https://doi.org/10.3390/w12010200, 2020.

Huang, S. Z., Chang, J. X., Huang, Q., Chen, Y. T., and Leng, G.Y.: Quantifying the relative contribution of climate and human impacts on runoff change based on the Budyko hypothesis and SVM model, Water Resour. Manag., 30(7), 2377–2390, https://doi.org/10.1007/s11269-016-1286-x, 2016a.

385   Huang, S., Huang, Q., Chang, J.X., and Leng, G. Y.: Linkages between hydrological drought, climate indices and human

activities: a case study in the Columbia River basin, Int. J. Climatol., 36(1), 280–290, https://doi.org/10.1002/joc.4344, 2016b.

Huang, S., Huang, Q., Leng, G.Y., and Chang, J. X.: A hybrid index for characterizing drought based on a nonparametric kernel estimator, J. Appl. Meteorol. Climatol., 55(6), 1377–1389, https://doi.org/10.1175/JAMC-D-15-0295.1, 2016c.

IPCC.: Climate Change 2021: The Physical Science Basis, Working Group I contribution to the Sixth Assessment Report of the Intergovernmental Panel on Climate Change, Masson-Delmotte, V., Zhai, P., Pirani, A., Connors, S. L., Péan, C., Berger, S., Caud, N., Chen, Y., Goldfarb, L., Gomis, M. I., Huang, M., Leitzell, K., Lonnoy, E., Matthews, J. B. R., Maycock, T. K., Waterfield, T., Yelekçi, O., Yu, R., and Zhou, B. (Eds.). Cambridge University Press, Cambridge, United Kingdom and New York, NY, USA, In press, https://doi.org/10.1017/9781009157896, 2021.

Jiang, Q., Li, W., Wen, J., Fan, Z., Chen, Y., Scaioni, M., and Wang, J.: Evaluation of satellite-based products for extreme rainfall estimations in the eastern coastal areas of China, J. Integr. Environ. Sci., 16(1), 191–207, https://doi.org/10.1080/1943815X.2019.1707233, 2019.

Jin, S. Y., Guo, S. M., and H, W. B.: Analysis on the Return Period of "7.20" Rainstorm in the Xiaohua Section of the Yellow River in 2021, Water, 14(15), 2444, https://doi.org/10.3390/w14152444, 2022.

Kebede, S. Y., Endalamaw, T. N., Sinshaw, G. B., and Atinkut, B. H.: Modeling soil erosion using RUSLE and GIS at watershed level in the upper beles, Ethiopia, Environ. Challenges, 2, 100009, https://doi.org/10.1016/j.envc.2020.100009, 2021.

Kilic, O. M. and Gunal, H.: Spatial-temporal changes in rainfall erosivity in Turkey using CMIP5 global climate change scenario, Arabian J. Geosci., 14, 1079, https://doi.org/10.1007/s12517-021-07184-2, 2021.

Kinnel, P. I. A.: Rainfall intensity-kinetic energy relationships for soil loss prediction, Soil Sci. Soc. Am. J., 45(1), 153–155, https://doi.org/10.2136/sssaj1981.03615995004500010033x, 1981.

Kite, G. W.: Confidence limits for design events, Water Resour. Res., 11(1): 48–53, https://doi.org/10.1029/WR011i001p00048, 1975.

Klik, A., and Rosner, J.: Long-term experience with conservation tillage practices in Austria: Impacts on soil erosion processes, Soil Tillage Res., 203, 104669, https://doi.org/10.1016/j.still.2020.104669, 2020.

Kong, F., Lu, L. L., and Fang, J.: Spatiotemporal pattern of hourly heavy rainfall in China and its spatial correlation with urbanization factors during 1991–2010, Climatic and Environmental Research (in Chinese), 22(3): 355–364, 10.3878/j.issn.1006–9585.2017.16139, 2017.

Liu, B. Y., Zhang, K. L., and Xie, Y.: An empirical soil loss equation. Proceedings-Process of Soil Erosion and Its Environment Effect, 2, 21–25, 2002.

Li, J., Liu, Z. H., and Li, R.: Temporal and spatial characteristics of rainfall erosivity with different geomorphology types on the loess plateau, Bull. Soil Water Conserv. (in Chinese), 28(3), 124–127, https://doi.org/10.13961/j.cnki.stbctb.2008.03.025, 2008.

Liu, S. Y., Huang, S. Z., Huang, Q., Xie, Y. Y., Leng, G. Y., Luan, J. K., Song, X. Y., Wei, X., and Li, X. Y.: Identification of the non-stationarity of extreme precipitation events and correlations with large-scale ocean-atmospheric circulation patterns: A case study in the Wei River Basin, China, J. Hydrol., 548, 184–195, https://doi.org/10.1016/j.jhydrol.2017.03.012, 2017.

Liu, S. L., Huang, S. Z., Xie, Y. Y., Leng, G. Y., Huang, Q., Wang, L., and Xue, Q.: Spatial-temporal changes of rainfall erosivity in the loess plateau, China: Changing patterns, causes and implications, Catena, 166, 279–289, https://doi.org/10.1016/j.catena.2018.04.015, 2018.

Liao, X., Xu, W., Zhang, J., Li, Y., and Tian, Y.: Global exposure to rainstorms and the contribution rates of climate change and population change, Sci. Total Environ., 663, 644–653, https://doi.org/10.1016/j.scitotenv.2019.01.290, 2019.

McGregor, K. C., Bingner, R. L., Bowie, A. J., and Foster, G. R.: Erosivity index values for northern Mississippi, Trans. ASAE, 38(4), 1039–1047, https://doi.org/10.13031/2013.27921, 1995.

Meusburger, K., Steel, A., Panagos, P., Montanarella, L., and Alewell, C.: Spatial and temporal variability of rainfall erosivity factor for Switzerland, Hydrol. Earth Syst. Sci., 16, 167–177, https://doi.org/10.5194/hess-16-167-2012, 2012.

430 Nearing, M. A., Pruski, F. F., and O'Neal, M. R.: Expected climate change impacts on hillslope erosion rates: a review, J. Soil Water Conserv., 59, 43–50, 2004.

Palharini, R. S. A., Vila, D. A., Rodrigues, D. T., Quispe, D. P., Palharini, R. C., de Siqueira, R. A., and de Sousa Afonso, J. M.: Assessment of the extreme precipitation by satellite estimates over South America, Remote Sens., 12(13), 2085, https://doi.org/10.3390/rs12132085, 2020.

435 ~~Petek, M., Mikoš, M., and Bezak, N.: Rainfall erosivity in Slovenia: Sensitivity estimation and trend detection, Environ. Res., 167, 528–535, https://doi.org/10.1016/j.envres.2018.08.020, 2018.~~

Panagos, P., Ballabio, C., Borrelli, P., Meusburger, K., Klik, A., Rousseva, S., Tadic, M. P., Michaelides, S., Hrabalikova, M., Olsen, P., Aalto, J., Lakatos, M., Rymszewicz, A., Dumitrescu, A., Begueria, S., and Alewell, C.: Rainfall erosivity in Europe, Sci. Total Environ., 511, 801–814, https://doi.org/10.1016/j.scitotenv.2015.01.008, 2015.

440 Panagos, P., Borrelli, P., Matthews, F., Liakos, L., Bezak, N., Diodato, N., and Ballabio, C.: Global rainfall erosivity projections for 2050 and 2070, J. Hydrol., 610, 127865, https://doi.org/10.1016/j.jhydrol.2022.127865, 2022.

Petek, M., Mikoš, M., and Bezak, N.: Rainfall erosivity in Slovenia: Sensitivity estimation and trend detection, Environ. Res., 167, 528–535, https://doi.org/10.1016/j.envres.2018.08.020, 2018.

Qian, H. W., Kong, H. J., Zhao, P. J., Ren, J. J., and Zhang, Y. Y.: Anomaly-based versus full-field-based weather analysis on 445 the extraordinary storm in Henan province in July 2021. Chinese J. Geophys. (in Chinese), 65(11): 4208–4224, https://doi.org/10.6038/cj92022P0631, 2022.

Rahmawati, N., and Lubczynski, M. W.: Validation of satellite daily rainfall estimates in complex terrain of Bali Island, Indonesia, Theor. Appl. Climatol., 134, 513–532, https://doi.org/10.1007/s00704-017-2290-7, 2018

Renard, K. G., Foster, G. R., Weesies, G. A., McCool, D. K., and Yoder, D. C.: Predicting soil erosion by water: a guide to 450 conservation planning with the revised universal soil loss equation (RUSLE), Agriculture Handbook, US Department of Agriculture, Washington, D. C., 1997.

Sadeghi, S. H., Hazbavi, Z., Zabihi, M., Larionov, G. A., Krasnov, S. F., Gorobets, A. V., Levi, Y., Erpul, G., Birkel, C., Hoyos, N., Naipal, V., Oliveira, P. T. S., Bonilla, C. A., Meddi, M., Nel, W., Al Dashti, H., Boni, M., Diodato, N., Van Oost, K., Nearing, M., and Ballabio, C.: Global rainfall erosivity assessment based on high-temporal resolution rainfall records. Sci. 455 Rep., 7, 4175, https://doi.org/10.1038/s41598-017-04282-8, 2017.

Shepard, D.: A two-dimensional interpolation function for irregularly-spaced data, Proceedings of the 1968 23rd ACM National Conference, ACM:517–524, 1968.

USDA-ARS.: Science documentation: Revised universal soil loss equation version2 (RUSLE2), US Department of Agriculture, Agricultural Research Service, Washington, D.C., 2013.

460 Viessman Jr., W. and Lewis, G.: Introduction to hydrology. Pearson Education Inc, San Antonio, U.S.A, 2002.

Wang, J. Q., and Luo, C. C.: Research on the characteristics of rainstorms and floods in China, Journal of China Hydrology (in Chinese), 26(3), 33–36, https://doi.org/10.3969/j.issn.1000-0852.2006.03.009, 2006.

Wang, W. T., Yin, S. Q., Xie, Y., Liu, B. Y., and Liu, Y. N.: Effects of four storm patterns on soil loss from five soils under natural rainfall, Catena, 141, 56–65, https://doi.org/10.1016/j.catena.2016.02.019, 2016.

465 Wang, W., Yin, S. Q., Gao, G., Papalexiou, S. M., and Wang, Z.: Increasing trends in rainfall erosivity in the Yellow River basin from 1971 to 2020, J. Hydrol., 610, 127851, https://doi.org/10.1016/j.jhydrol.2022.127851, 2022.

Wischmeier, W. H. and Smith, D. D.: Rainfall energy and its relationship to soil loss, Trans. Am. Geophys. Union, 39, 285–291, https://doi.org/10.1029/TR039i002p00285, 1958.

Wischmeier, W. H. and Smith, D. D.: Predicting rainfall erosion losses from cropland east of the Rocky Mountains, Agriculture

470   Handbook, US Department of Agriculture, Washington, D. C., 1965.

Wischmeier, W. H. and Smith, D. D.: Predicting rainfall erosion losses: A guide to conservation planning, Agriculture Handbook, US Department of Agriculture, Washington, D. C., 1978.

Yin, S. Q., Nearing, M. A., Borrelli, P., and Xue, X. C.: Rainfall Erosivity: An Overview of Methodologies and Applications, Vadose Zone J., 16(12), https://doi.org/10.2136/vzj2017.06.0131, 2017.

475   Yin, S., Xue, X., Yue, T., Xie, Y. and Gao, G.: Spatiotemporal distribution and return period of rainfall erosivity in China, Trans. Chinese Soc. Agric. Eng. (in Chinese), 35, 105–113, https://doi.org/1002-6819(2019)35:9<105:ZGJYQS>2.0.TX;2-W, 2019.

Yue, T. Y., Xie, Y., Yin, S. Q., Yu, B. F., Miao, C. Y., and Wang, W. T.: Effect of time resolution of rainfall measurements on the erosivity factor in the USLE in China, ISWCR, 8, 373–382, https://doi.org/10.1016/j.iswcr.2020.06.001, 2020.

480   Yue, T. Y., Yin, S. Q., Xie, Y., Yu, B. F., and Liu, B. Y.: Rainfall erosivity mapping over mainland China based on high-density hourly rainfall records, Earth Syst. Sci. Data, 14, 665–682, https://doi.org/10.5194/essd-14-665-2022, 2022.

Zhang, X., Yang, H., Wang, X. M., Shen, L., Wang, D., and Li, H.: Analysis on characteristic and abnormality of atmospheric circulations of the July 2021 extreme precipitation in Henan, Trans. Atmos. Sci. (in Chinese), 44(5), 672–687, https://doi.org/10.13878/j.cnki.dqkxxb.20210907001, 2021.

485   Zhang, X. K., Feng, L. C., and Cui, X. L.: Study on urban resilient waterlogging control system under 7.20 rainstorm in Zhengzhou — Core area of Fuzhou Binhai New Town, J, Catastrophol. (in Chinese), 37(2), 79–83, https://doi.org/10.3969/j.issn.1000811X.2022.02.014, 2022.

Zhou, P. H. and Wang, Z. L.: A study on rainstorm causing soil erosion in the Loess Plateau, J Soil Water Conserv. (in Chinese), 6(3), 1–5, https://doi.org/10.13870/j.cnki.stbcxb.1992.03.001, 1992.

490   Zhang, X., Yang, H., Wang, X. M., Shen, L., Wang, D., and Li, H.: Analysis on characteristic and abnormality of atmospheric circulations of the July 2021 extreme precipitation in Henan, Trans. Atmos. Sci. (in Chinese), 44(5), 672–687, https://doi.org/10.13878/j.cnki.dqkxxb.20210907001, 2021.

Zhang, X. K., Feng, L. C., and Cui, X. L.: Study on urban resilient waterlogging control system under 7.20 rainstorm in Zhengzhou — Core area of Fuzhou Binhai New Town, J, Catastrophol. (in Chinese), 37(2), 79–83,
495   https://doi.org/10.3969/j.issn.1000811X.2022.02.014, 2022.